G-SC-IRSA: Graph-based Spatially Coupled IRSA for Age-Critical Grant-Free Massive Access

Yuhao Huang, Jian Jiao, *Member, IEEE,* Ye Wang, *Member, IEEE,* Shaohua Wu, *Member, IEEE,* Rongxing Lu, *Fellow, IEEE* and Qinyu Zhang, *Senior Member, IEEE*

***Abstract*—In this paper, we focus on a grant-free massive access setup and analyze its age of information (AoI), where a large number of user equipments (UEs) are randomly activated and attempt transmitting status update packets to a base station (BS) over a common shared channel. To support this age-critical grant-free massive access, we propose a graph-based spatially coupled irregular repetition slotted ALOHA (G-SC-IRSA) random access protocol, which utilizes the pseudo-random access pattern (PRAP), coupled frames, and sliding window decoder (SWD) to improve the packet loss rate (PLR) and AoI performance. Specifically, we derive the approximate expressions to the normalized average AoI (AAoI) as a function of the PRAP and system load. Then, we establish the problem of minimizing the AAoI under the G-SC-IRSA protocol. Furthermore, we utilize the density evolution (DE) with a bipartite graph to evaluate the system load threshold of G-SC-IRSA in asymptotic regime, and achieve an optimal degree distribution via the differential evolution algorithm, and finally obtain the optimal PRAP with PEG algorithm. Simulation results validate the accuracy of our theoretical derivations, and show the G-SC-IRSA can achieve the minimum AAoI with the optimal PRAP, and outperforms the existing benchmark schemes in terms of PLR and AAoI.**

***Index Terms*—Age of information, pseudo-random access pattern, massive access, grant-free, sliding window decoder.**

I. Introduction

INTERNET of Things (IoT) is a well-known paradigm for future communication systems, and has been widely studied in industry and academia [1]–[3]. One of its key scenarios is massive machine-type communication (mMTC), in which a massive number of user equipments (UEs) transmit short data packets to the base station (BS) over a common shared channel with low energy consumption [4]. In such a case, the conventional 4-step handshake scheme (e.g., LTE-A) brings significant delay, and the grant-free scheme, where UEs use a contention-based approach to access without being scheduled by the BS, which simplifies the handshake procedure to 2-step RACH, has been extensively studied and is well suited for massive access [5]–[7].

Slotted ALOHA [8] is the earliest grant-free random access protocol, with the normalized throughput bottleneck $1/e \approx 37\%$ when the number of UEs approaches infinity [9]. To break through the bottleneck of slotted ALOHA, a recent class of schemes called *modern random access protocols* [10], which are inspired from the low-density parity-check (LDPC) code and successive interference cancelation (SIC) receiver, has been proposed. The irregular repetition slotted ALOHA (IRSA) protocol is a relevant example [11], and the performance is analyzed in [12]–[14]. In [11], the authors first organize M slots into a medium access control (MAC) frame. Then, the UEs transmit packet replicas multiple times according to a repetition distribution, and the BS performs the SIC to decode the replicas. Each frame forms a coding pattern, and recovered by SIC receiver, which allows IRSA to achieve near 100% normalized throughput in asymptotic analysis. With the perfect asymptotic performance, the authors in [13], [14] are more concerned with the performance at short frame lengths, in which case IRSA only achieves a normalized throughput of approximately 0.8.

Subsequent works firstly include applying the IRSA to the asynchronous case [15] and half-duplex broadcast network [16], and other works focus on further improving the packet loss rate (PLR) performance of IRSA in finite frame length [11], [17]–[19]. In [17], the authors propose a pseudo-random access scheme in IRSA, which achieves a lower error floor than the standard IRSA. In [18], the authors propose a coupling approach to enhance the performance of random access, and derive a theoretical bound for the scheme.

Parallel to the development of grant-free protocol, researchers are increasingly concerned the timeliness of information in random access, which is measured by the age of information (AoI) [20]–[26]. This metric is defined by giving equal importance for all packets, and the receiver measuring the freshness information with the gap between the time-stamp of the latest received packet [20]. On one hand, maximizing the throughput or minimizing delay can not fully guarantee the freshness of information, and a related indicator of AoI can be utilized to describe the overall freshness performance of massive access at BS, named average AoI (AAoI) [21]. On the other hand, in the above frame-based protocols, i.e., IRSA and frameless ALOHA with their enhanced version, the latency cannot measure the timeliness of the whole system. As a result, we should also study the AAoI performance for

Manuscript received xxx, 2022. This work was supported in part by the National Natural Sciences Foundation of China (NSFC) under Grant 62071141, Grant 61871147, Grant 61831008, and Grant 62027802, in part by the Shenzhen Science and Technology Program under Grant JSGG20220831110801003 and Grant GXWD20201230155427003-20200822165138001, and in part by the Major Key Project of PCL Department of Broadband Communication. (*Corresponding author: Jian Jiao.*)

Yuhao Huang, Jian Jiao, Shaohua Wu, and Qinyu Zhang are with the Guangdong Provincial Key Laboratory of Aerospace Communication and Networking Technology, Harbin Institute of Technology (Shenzhen), Shenzhen 518055, China, and also with Peng Cheng Laboratory, Shenzhen 518055, China (e-mail: 20s152118@stu.hit.edu.cn; jiaojian@hit.edu.cn; hitwush@hit.edu.cn; zqy@hit.edu.cn).

Ye Wang is with Peng Cheng Laboratory, Shenzhen 518055, China (e-mail: wangy02@pcl.ac.cn).

Rongxing Lu is with the Faculty of Computer Science, University of New Brunswick, Fredericton, NB E3B 5A3, Canada, (e-mail: rlu1@unb.ca).

the grant-free IRSA protocol in age-critical scenarios.

For AoI in massive access, a category of work focuses on the threshold ALOHA [22], [23]. The authors in [22], [23] propose that the UE can access only when the AoI is greater than a certain threshold, which indirectly controls the interval between the UE transmitting two update packets, thereby reducing the AoI. However, these works only consider the access with a small number of UEs. Another category of work, which is more relevant to our paper, discusses the AoI performance of the IRSA protocol. In [24], the authors propose a random access model, when UEs are activated according to a stochastic process, they sample the packets and transmit them in the next frame. In this setting, the authors obtained the closed-form expression of AAoI, and further used the Markov chain in [25] to analyze the specific AAoI behavior and age-violation probability in the IRSA protocol. They are the first works analyzing the AAoI performance of IRSA, but the minimization of AAoI in IRSA is not considered in [24], [25]. The authors in [26] consider the fixed number of activated UEs, and divide them into two types according to the sampling time point for each UEs. The main method for optimizing AAoI is to recover packets early in a frame, called the "REARLY-n" strategy in [26]. This work does not consider activation models and massive access.

In this paper, we simplify the activation model in [24] to suit the grant-free protocols, and we propose a novel G-SC-IRSA protocol with higher throughput and lower AAoI performance. Specifically, our contributions are as follows.

- We consider a sparse massive access model with a large number of UEs and a small activation probability, where the packets are generated at the start of a frame and packet decoding is performed at the end of the frame. In this model, we propose G-SC-IRSA protocol with a pseudo-random access pattern (PRAP), coupled frames, and sliding window decoder (SWD) to improve throughput and reduce AAoI. We design and optimize a fixed PRAP matrix to lower the PLR, and introduce the coupled frames to further lower the AAoI.
- We derive an approximate analytical expression for the AAoI of the G-SC-IRSA protocol, which is characterizing the AAoI as a function of the system load and the PRAP. Based on this expression, we propose the problem of minimizing AAoI under the sparse massive access model. To solve the optimization problem, we first divide the protocol into two cases according to the length of the coupled frame, named G-SC-2 and G-SC-F, respectively.
- Moreover, we develop a fundamental framework for analysis, design and optimization of PRAP. Specifically, we propose two novel random access protocols, named SC-2 and SC-F, respectively, and utilize the density evolution (DE) to analyze the asymptotic performance. Then, we obtain the optimal degree distribution via the differential evolution algorithm for both two settings, and finally utilize the progressive edge-growth (PEG) algorithm [27], [28] to generate optimal PRAP. Simulation results show that our G-SC-IRSA can achieve the minimum AAoI with the optimal PRAP, and all the performances of two cases are better than that of standard IRSA.

The remainder of the paper is organised as follows. We start our work in Section II by introducing the system model and describing our G-SC-IRSA protocol. To measure the freshness of proposed protocol, we first describe the AoI model, analyze the AAoI performance, and establish the problem of minimizing AAoI in Section III. We mainly utilize the DE to analyze the asymptotic behavior of protocol in Section IV. The numerical results are given in Section V. Finally, conclusions are drawn in Section VI.

II. System Model and G-SC-IRSA Protocol

We consider a typical synchronous slot random access scheme, where M consecutive slots are organized in medium access control (MAC) frames, and M is the frame length. All UEs and the BS are frame and slot synchronous with each other, and a UE schedules at most one packet transmission in a frame. In this paper, the collision channel is used as the channel model [12]–[14]. Accordingly, the BS receives the superimposed signal from multiple UEs in each slot, and the BS can identify the following three situations according to the received signal power: a) *Silence*, there is no activated UE transmitting in this slot; b) *Singleton*, there is a single UE transmitting replica in this slot, where the slot is called singleton slot; c) *Collision*, multiple UEs transmit replicas in this slot, and a collision occurs. To simplify the analysis, when a singleton slot is detected by BS, it will always be successfully decoded. When a collision is detected, any information in the slot will not be decoded.

In this system, the setting of the mMTC scenario is that, i.e., a) N potential UEs access the BS with a common shared channel, where $N \gg M$; b) The activated UEs are defined as UEs who have a transmission plan at the beginning of the frame, and these UEs will buffer the scheduled packets for transmitting the packet replicas. In each access frame, only a small number of activated UEs and transmit packet replicas to the BS, which is described by the activation probability π. Since every UE is independently activated in each access frame, the number of activated UEs in a frame N_a can be modeled as a binomial distribution with expected $\mathbb{E}[N_a] = \pi N$. At the same time, the system load G can be defined as the number of packets transmission per slot:

$$G = \frac{\mathbb{E}[N_a]}{M} = \frac{\pi N}{M}. \tag{1}$$

These two characteristics respectively correspond to the requirements of massive access and sporadic burst transmission in the mMTC scenario.

Then, we will describe our proposed G-SC-IRSA protocol from two aspects, i.e., the pseudo-random access method and the coupled frame. In the initialization, the BS can assign unique IDs to all potential UEs to support the pseudo-random access method. Since a UE is assigned an ID, we use subscript i to indicate the UE as U_i.

A. Pseudo-Random Access Method

In this subsection, we introduce how the UEs use their own ID and access offset (AO) to select slots to transmit packet

This article has been accepted for publication in IEEE Internet of Things Journal. This is the author's version which has not been fully edited and content may change prior to final publication. Citation information: DOI 10.1109/JIOT.2022.3232568

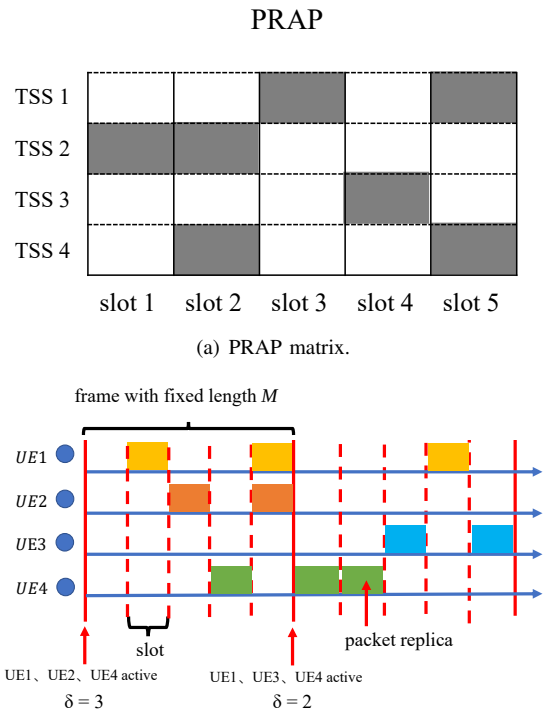

(a) PRAP matrix.

(b) The transmitting pattern of all UEs and AO.

Fig. 1. An example of selection transmitting slots based on PRAP and AO.

replicas. The BS broadcasts a beacon for synchronization at the beginning of every frame, and also broadcasts an AO δ_k, where the subscript k means the k-th frame. When the activated UEs receive the AO, they select their own transmitting slot sequence (TSS) to transmit packet replicas in the fixed PRAP matrix according to their own ID and AO δ_k. An example of determining the transmitting slot based on PRAP and AO is shown in Fig. 1. Note that when a transmission frame is completed, the UEs would buffer this packet to transmit coupled packet mentioned in Sec. II-B. The TSS is a binary sequence denoted as

$$S = [s_1, \ldots, s_i, \ldots, s_M],$$

where the UE plans to transmit a packet replica in the i-th slot of the frame if $s_i = 1$, called transmitting slot. We can calculate the transmitting times with its l_0 norm $\|S\|_0$. The PRAP is a binary matrix, containing N TSS, corresponding to N potential UEs, denoted by

$$P = \begin{bmatrix} S_1 \\ \vdots \\ S_j \\ \vdots \\ S_N \end{bmatrix} = \begin{bmatrix} s_{1,1}, & \ldots & s_{1,i}, & \ldots & s_{1,M} \\ \vdots & \ddots & \vdots & \ddots & \vdots \\ s_{j,1}, & \ldots & s_{j,i}, & \ldots & s_{j,M} \\ \vdots & \ddots & \vdots & \ddots & \vdots \\ s_{N,1}, & \ldots & s_{N,i}, & \ldots & s_{N,M} \end{bmatrix}$$

where j is the index number of TSS in this PRAP. It is worth noting that P is a sparse matrix, predetermined and buffered in all potential UEs and BS, and determines the transmitting slot selection of all potential UEs behavior[1]. A row of matrix P is a TSS, which means that the UE choosing this row needs to select transmitting slots according to the TSS.

Let $j = (i + \delta_k) \mod N$, and the UE U_i selects the TSS in the following way:

$$j^\dagger = \begin{cases} j, & j > 0, \\ N, & j = 0, \end{cases} \tag{2}$$

where $j^\dagger$ is the index number of TSS selected by the UE U_i. It can be seen that the same UE will select different TSSs under different AO to ensure the randomness of the access process. This involves the design of the AO sequence $\{\delta_k\}$. Here we choose the pseudo-random sequence and ensure that the two adjacent AOs must be different[2], i.e., $\forall k, \delta_k \neq \delta_{k+1}$, which can ensure that the same UE selects different TSSs in adjacent frames.

Next, we will give an example of determining the transmitting slot based on PRAP and AO. There are $N = 4$ potential access UEs in the system, and $M = 5$ i.e., a frame with 5 slots, as shown in Fig. 1. Fig. 1(a) shows the PRAP of the system, and Fig. 1(b) shows the transmitting frame of all UEs. In the first and second frames, the AO broadcast by the BS is $1, 3$, and UE1, UE2, UE4 and UE1, UE3, UE4 are activated respectively. The activated UEs select the TSS from the PRAP according to the AO and their own ID, according to Eq. (2). For example, in the first frame, UE2 is activated with $id = 2, \delta_1 = 3$, so it selects the first TSS, i.e., UE2 transmits the replicas on slot3 and slot5. All UEs use this method to transmit packet replicas.

B. The Coupled Frame

One of the main contributions of this paper is to propose a coupled method to improve performance. Different from [18], which considers a convolutional super-frame structure, we design the coupling between MAC frames. First, we introduce the process of coupled frame. In our system model, when the transmission of the current frame is completed and the transmission of the next frame is about to start, there is a type of UEs, which is activated and transmits packet replicas in these two frames. Recall that these activated UEs satisfy the binomial distribution and the activated probability is π. It can be known that the proportion of this type of UEs in activated UEs is approximately π^2/π, and we call this type of UEs type-π UEs.

[1]Note that in [17], the BS directly allocates TSS to each UEs, and UEs do not need to store the entire PRAP. In our protocol, since the UEs store the entire PRAP, the BS only needs to assign an ID to each UEs, and UEs choose the TSS according to the ID and AO, where part of the calculation is transferred to the UEs, and it improves the reliability of transmission in initialization step. Although storing the entire PRAP reduces a part of the computing cost, it requires more storage space. A structured PRAP can then be constructed to achieve a trade-off between storage and performance, such as the QC LDPC matrix used in 5G. Further, we can optimize the matrix in advance, and the UEs can utilize the corresponding indicator to construct the TSS to reduce the complexity.

[2]In fact, AO is only used to improve the security performance of the proposed protocol and has no effect on the PLR and AoI performance. The AO used by UEs in the two frames are different, which ensure that the TSS sent in the two frames are different, so as to ensure that there is no correlation, and prevent forward leakage.

This article has been accepted for publication in IEEE Internet of Things Journal. This is the author's version which has not been fully edited and content may change prior to final publication. Citation information: DOI 10.1109/JIOT.2022.3232568

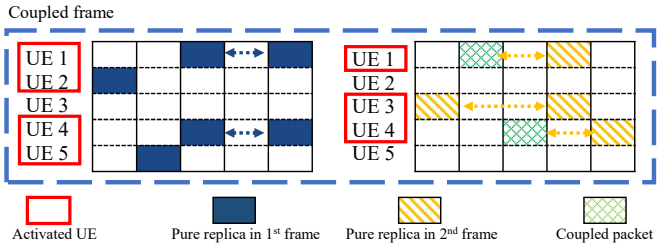

Fig. 2. An example of a coupled frame. Solid rectangles, shaded rectangles, and cross-shaded rectangles indicate pure replicas in first frame, pure replicas in second frame, and coupled packets, respectively. Dotted lines indicate pointers between replicas of the same UE

Type-π UEs will select a transmitting slot in TSS with uniform distribution to transmit the coupled packet. When the next transmission frame ends, these two frames, marked as the first frame and the second frame, form a coupled frame with a frame length of 2, denoted as $l_c = 2$. The coupled packet includes the modulo-2 sum of the pure packet replicas (i.e., uncoupled packet replicas) in the first frame and that in the second frame.

It can be known that when the coupled frame length is l_c, the activated UE in the first frame always transmits pure replicas, and the following $l_c - 1$ frames all have type-π UEs and they transmit coupled packets. Note that the type-π UEs between two consecutive frames may not be the same, but the total number of these type of UEs is almost the same, about $\pi^2 N$. It is foreseeable that the coupled length l_c has a strong correlation with the performance of the proposed protocol. Therefore, we mainly focus on two cases of l_c:

- $l_c = 2$. It characterizes the performance of the protocol, where there exist coupled packets every other frame. This is the start point for our research on coupled frames and we denote this case as G-SC-2.
- $l_c = \infty$. This case is equivalent to the situation, where there are coupled packets in all frames except the first frame. This is also the asymptotic performance of the protocol performance as the coupled length l_c increases. We denote this case as G-SC-F.

The specific protocols corresponding to the above two cases are shown in Fig. 5(a) and Fig. 5(b), respectively. The only difference between the two cases is that the coupled length is different, and the G-SC-2 case is also the basis for our research on G-SC-F case.

An example of coupled frame is shown in Fig. 2. Suppose $N = 5$ and $M = 5$, and the coupled length l_c is 2, where UE1, UE2, UE4 and UE5 are activated in the first frame, and UE1, UE3 and UE4 are activated in the second frame, so the UE1 and UE4 are type-π UEs and will transmit coupled packets, i.e., modulo-2 sum packets in the second frame. Specifically, UE1 and UE4 transmit this type of packets on the first transmitting slot (i.e. slot 2, slot 3), and transmit pure replicas on other slots in the second frame[3].

[3]In this example, UE1 and UE4 both have 0.5 probability of choosing another transmitting slot, which is slot 4 and slot 5, respectively.

C. The Structure of Sliding Window Decoder

In the standard IRSA, the BS performs SIC process for decoding. However, in the proposed G-SC-IRSA protocol, due to the existence of the coupled packets, the decoder equipped at the BS also needs to be replaced accordingly. In the paper, the BS performs SWD. In order to perform SWD at the BS for decoding, we suppose that for UEs:

- Each UE can buffer at most 2 packets. For G-SC-2 case, it is sufficient for the UE to buffer 2 pure packets to transmit coupled packets; For G-SC-F case, buffering coupled packets and new pure packets is also sufficient to transmit new coupled packets. Note that the probability of the same UE transmitting three or more coupled packets successively is very small, and the probability of transmitting three coupled packets is π^3.
- Each replica contains identification information to mark whether it is a pure replica or a coupled packet;
- The pure replica contains a pointer to the other replica within a frame, and the coupled packet additionally contains pointers to all replicas of the previous frame[4].

For BS, we suppose that:

- The BS buffers at most 2 frames. In the following, we mention that the window length of SWD $l_d = 2$, so buffering 2 frames is sufficient;
- Corresponding to the behavior of the UE, after the BS successfully decodes a packet, the BS can identify the pure replica and the coupled packet, and then find the slot with the pointers contained in it.

Under the above assumptions, the coupled frame shown in Fig. 2 appears on the SWD as two orthogonal pure frame areas, and a connected coupled area as shown in Fig. 3. Meanwhile, the packets in coupled area have pointers to the previous frame, which makes these packets behave similarly to the pure packets in the first frame with SIC process as shown in Fig. 4. Specifically: a) When the pure packet in the first frame transmitted by the same UE is decoded, the packet in the coupled area is also decoded if exists[5]; b) When the packet in the coupled area is decoded[6], the packet on the first frame transmitted by the same UE can also be decoded according to the assumptions 2 for BS. According to the above argument, the coupled packets transmitted by type-π UEs in the second frame can be disassembled into two independent pure packets on the same slot.

Then, we first emphasize the characteristics of SWD, including sliding outside the window, and performing the standard SIC process inside the window. The number of frames occupied by the window of SWD is defined as the window length l_d. The relationship between the window length l_d and the

[4]In our pseudo-random access method, one way to achieve this is to use AO received previous and PRAP to quickly generate pointers to TSS in the previous frame.

[5]At this time, the BS stores the data of pure packet in the first frame, and when the coupled packet transmitted by the same UE is also decoded, the BS calculates the data of the pure packet on the second frame through the modulo two sum.

[6]This situation occurs when the pure replicas sent by a UE on the second frame is successfully decoded, resulting in that only a single packet exists on this slot in the coupled area.

This article has been accepted for publication in IEEE Internet of Things Journal. This is the author's version which has not been fully edited and content may change prior to final publication. Citation information: DOI 10.1109/JIOT.2022.3232568

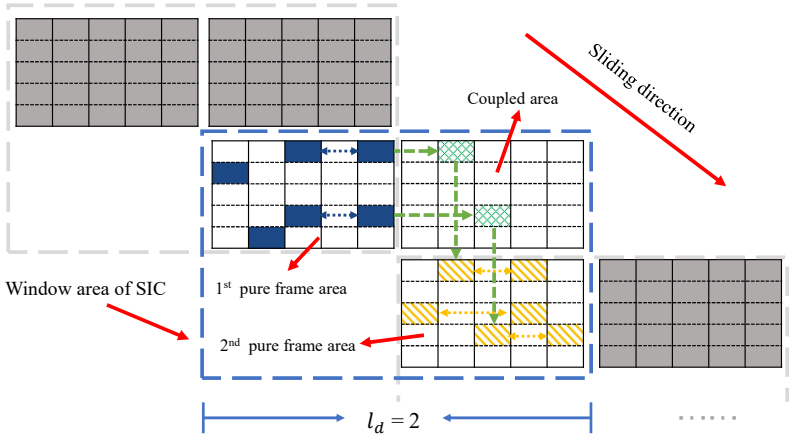

(a) The structure of coupled frame and SWD

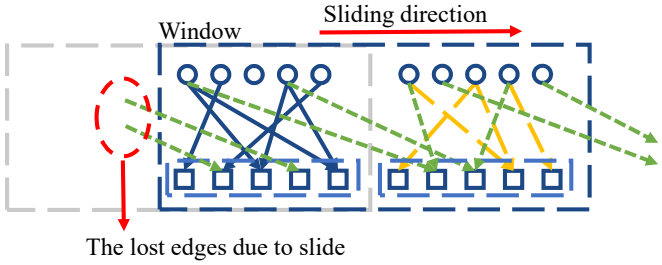

(b) Bipartite graph of coupled frame in SWD

Fig. 3. An example of coupled frame in SWD with $l_d = 2$ and its bipartite graph. Dotted lines indicate pointers between replicas of the same UE.

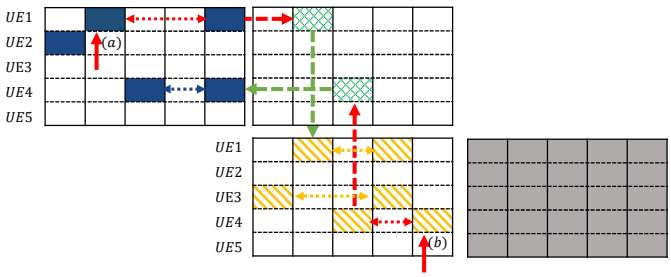

Fig. 4. An example of replicas decoded behavior between coupled area and pure frame areas

coupled length l_c will affect the performance of SWD. When $l_d > l_c$, some coupled packets that have not been decoded successfully will be discarded during the sliding process, thereby reducing the probability of successful decoding as shown in Fig. 3(b) with red circle. Note that we only consider the situation when $l_d = 2$ in the paper. For the two cases mentioned in Sec. II-B, SWD has the following conditions:

- $l_c = l_d = 2$. In the sliding process of SWD, there are coupled packets in the coupled area one frame apart.
- $l_c = \infty, l_d = 2$. There are always coupled packets in the coupled area during the sliding process. Since $l_d = 2$, the decoding information of the previous frame will be lost every time it slides.

There are two reasons for two cases mentioned above, a) The window length is short so the decoding complexity is reduced. For the SC-2, the window length of 2 frames is sufficient. For the SC-F, compared with other window lengths, the performance gap is slight[7]. b) The decoding latency is relatively short, which is consistent with our demand for timeliness and delay, and the gain to AAoI can be seen in the later simulations in Sec. V.

III. AoI Model and AAoI Analysis

A. Age of Information in G-SC-IRSA protocol

To evaluate the ability to maintain the freshness of information for all UEs in this system, we denote the current AoI of the UE U_i as $A_i(t)$, where t is the slot index. We assume that $A_i(1) = 1, \forall i \in \{1, \ldots, N\}$, and $A_i(t)$ increases by one for each slot unless a successful decoding occurs. Denote the slot index of U_i sampling a packet by $T_x^{(i)}$ and BS decoding the packet by t. Recalling that U_i samples status at the beginning of the frame, which means $T_x^{(i)} \in kM + 1, k \in \mathbb{N}$. Thus, the evolution of the current AoI for U_i can be expressed as

$$A_i(t+1) := \begin{cases} A_i(t) + 1, & \text{if } U_i \text{ is not decoded at } t, \\ t - T_x^{(i)}, & \text{if } U_i \text{ is decoded at } t, \end{cases} \quad (3)$$

[7]Mentioned in [29], there is almost no loss in performance when the window length is more than 5 frames.

This article has been accepted for publication in IEEE Internet of Things Journal. This is the author's version which has not been fully edited and content may change prior to final publication. Citation information: DOI 10.1109/JIOT.2022.3232568

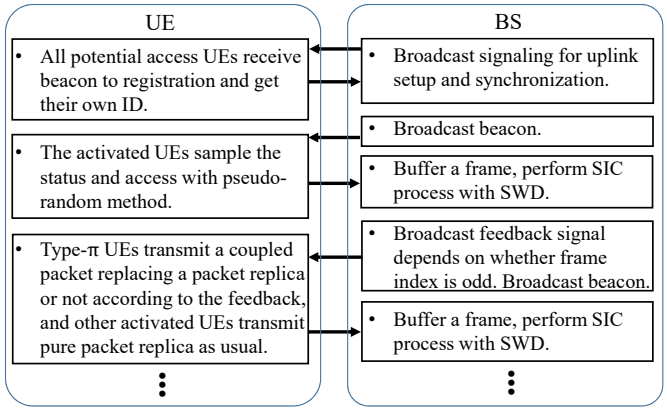

(a) Case #1: G-SC-2, the length of coupled frame is 2.

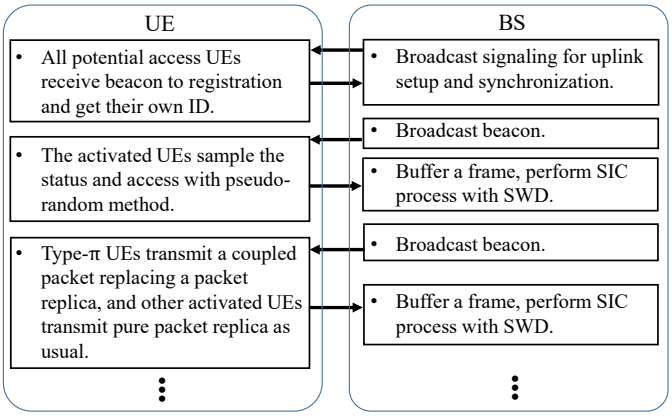

(b) Case #2: G-SC-F, the length of coupled frame is infinity, which means all the frame exist the coupled packets.

Fig. 5. Two cases of G-SC-IRSA with different coupled ways.

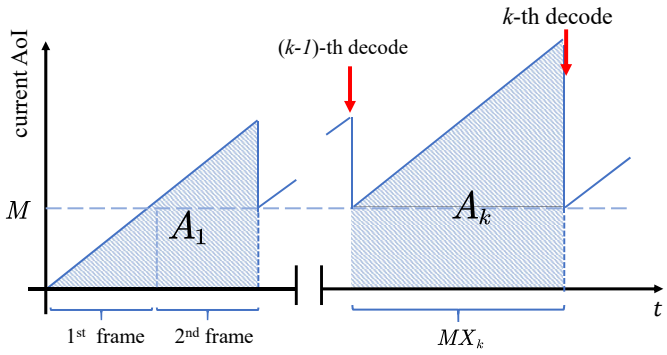

Fig. 6. Example timeline of current AoI of U_i. Between two decode process, the number of slots is described as MX_k, and the accumulated age is illustrated by shaded area and marked by A_k.

and the AAoI for U_i can be defined as

$$\bar{A}_i := \lim_{T\to\infty} \frac{1}{T} \sum_{t=0}^{T} A_i(t). \tag{4}$$

Due to the independent identically distributed ($i.i.d.$) operation of UEs in random access scheme, the AAoI of this system can be described as follows

$$\bar{A} = \frac{1}{N} \sum_{i=1}^{N} \bar{A}_i. \tag{5}$$

B. AAoI Analysis in G-SC-IRSA

Then, we derive the AAoI expression for UEs with random activation and IRSA to access, and it can be used to estimate the AAoI of the proposed G-SC-IRSA protocol[8], which is expressed as the following theorem:

Theorem 1. *In the G-SC-IRSA random access protocol with randomly activated UEs, the AAoI of system $\bar{A}$ is evaluated by*

$$\bar{A} = \frac{M}{2} + \frac{M}{\pi(1-P_e)} + \frac{1}{2}, \tag{6}$$

where P_e is the PLR of G-SC-IRSA and π is the activation probability of UEs. A bound of AAoI is that,

$$\bar{A} = \frac{M}{2} + \frac{M}{\pi} + \frac{1}{2}. \tag{7}$$

[8]The AoI update situation of G-SC-IRSA is more complicated, so we only make a rough estimate with IRSA. More precise expressions are left to future work

Proof: The evolution of the current AoI of U_i is shown in Fig. 6. Consider the slots index of the $(k-1)$-th and the k-th successful decoding, and denote the number of frames during this period by X_k. The curve of current AoI and the y-axis enclose a trapezoidal with height MX_k and its area is marked by A_k. The long-term average AoI of the U_i can be expressed as the ratio of the trapezoidal area to the height, and we have

$$\bar{A}_i = \lim_{k\to\infty} \frac{\sum_k A_k}{\sum_k MX_k}. \tag{8}$$

For IRSA operation, the current AoI of U_i will drop to M if decoded successfully. Thus, A_k can be calculated by M and X_k as follows,

$$A_k = \sum_{d=1}^{MX_k} M + d = M^2 X_k + MX_k(MX_k+1)/2, \tag{9}$$

where X_k obeys geometric distribution, satisfying $\Pr\{X = k\} = (1-p)^{k-1}p, k = 1, 2, \ldots$, where p is calculated by $p = \pi(1-P_e)$, which means the average packets decoded in a frame. The first and second moments of X_k can be expressed as $\mathbb{E}[X_k] = 1/p$ and $\mathbb{E}[X_k^2] = (2-p)/p^2$, and the AAoI of U_i can be calculated with Eq. (8) and (9) as follows

$$\begin{aligned}\bar{A}_i &= \lim_{k\to\infty} \frac{\sum_k M^2X_k + MX_k(MX_k+1)/2}{\sum_k MX_k} \\ &= M + \frac{M\mathbb{E}[X_k^2]}{2\mathbb{E}[X_k]} + \frac{1}{2} \\ &= \frac{M}{2} + \frac{M}{\pi(1-P_e)}\frac{1}{2}.\end{aligned} \tag{10}$$

Recalling that all U_i are activated and access independently, it means $\bar{A} = \bar{A}_i$ with Eq. (5), which proves the theorem. ■

C. Problem of Minimize AAoI

We also define the normalized AAoI, which describes the AoI performance without the effect of total number of UEs, marked as $\tilde{A}$ and shown as following,

$$\tilde{A} = \frac{\bar{A}}{N} \approx \frac{M}{2N} + \frac{1}{T}, \tag{11}$$

where T is the throughput of G-SC-IRSA and is defined as $T = G(1-P_e)$. The ratio of M to N is more critical in the analysis, so we let $\eta = M/N$ and we have[9]

$$\tilde{A} = \frac{\eta}{2} + \frac{1}{T}. \tag{12}$$

Recall that the system load G is defined as the ratio of the average number of activated UEs πN to frame length M, thus

$$G = \frac{\pi N}{M} = \frac{\pi}{\eta}, \tag{13}$$

where $G \in [0, 1]$, so $\pi \in [0, \eta]$. Based on Eq. (12), we describe the AAoI minimization problem under G-SC-IRSA as,

$$\min_{G,P} \frac{\eta}{2} + \frac{1}{T}, \tag{14}$$

[9]In fact, η can be considered as the rate of the LDPC code corresponding to PRAP matrix.

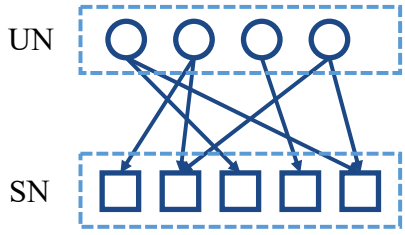

(a) Bipartite graph $\mathcal{G}_{\text{LDPC}}$ corresponding to PRAP.

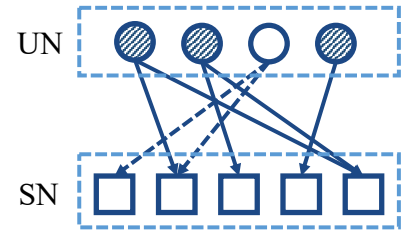

(b) Residual graph $\mathcal{G}_{\text{a}}$ during a transmission.

Fig. 7. An example of bipartite graph and residual graph. There is the bipartite graph $\mathcal{G}_{\text{LDPC}}$ corresponding to PRAP in (a), and a residual graph during a transmission $\mathcal{G}_{\text{a}}$ in (b). Shaded nodes in (b) represent UEs participating transmission. Since the relation of AO, the UNs in (b) is cyclically shifted, but does not affect the connection relation, so the two graphs are still isomorphic.

where P is the PRAP matrix. Select one of η and N as the pivot variable, and the other one changes accordingly. It can be seen that the AAoI is monotonically decreasing on any variable, and the problem is transformed to minimize AAoI under the given N and M. We leave the discussion on this minimization problem in Sec. V.

IV. Analysis of G-SC-IRSA Protocol

As mentioned above, the performance of G-SC-IRSA is affected by the parameter group (N, M, P, π, l_c, l_d), and a key issue is to find P to optimize the performance when l_c, l_d, N, M are fixed. In this section, we have followed the ideas in [17] by using bipartite graphs to build a bridge between the LDPC code and our PRAP, where we can find the corresponding PRAP with the given degree distribution $\Lambda(x)$ in asymptotic analysis. To find the optimal degree distribution in asymptotic analysis, we utilize the density evolution (DE) analysis for two settings respectively, and we use the result of DE and differential evolution algorithm to obtain the optimal degree distribution table under a given $d_{\max}$ for these two settings. The details of DE can be found in [11], [15], [16].

A. Design of PRAP Matrix

Recalling that in an LDPC code with N variable nodes (VNs) and M check nodes (CNs), the size of the parity check matrix is $N \times M$, and the corresponding bipartite graph is denoted as $\mathcal{G}_{\text{LDPC}}$. Consider the graph composed of N_a VNs and their neighbor CNs, called the residual bipartite graph, denoted as $\mathcal{G}_{\text{a}}$. Each round of transmission can be equivalent to generating a residual graph $\mathcal{G}_{\text{a}}$, and its SIC process is

equivalent to performing a BP iterative algorithm on this graph. In the example given in Fig. 1, the bipartite graph $\mathcal{G}_{\text{LDPC}}$ corresponding to PRAP and a residual graph during a transmission $\mathcal{G}_{\text{a}}$ (corresponding to AO = 3) is shown in Fig. 7. The girth (mostly length-4 and 6 cycles) in the residual graph $\mathcal{G}_{\text{a}}$ will affect the decoding of this SIC process [14]. Since the residual bipartite graph is a subgraph of $\mathcal{G}_{\text{LDPC}}$, we need to construct a longer girth bipartite graph $\mathcal{G}^*_{\text{LDPC}}$, and its parity check matrix H^* is the PRAP matrix.

Note that the VN and CN here correspond to the UE node (UN) and slot node (SN) of the G-SC-IRSA protocol, respectively, and we define the node-perspective degree distribution of UN (SN) as $\{\Lambda_l\}$ ($\{\text{P}_l\}$), where Λ_l (P_l) denotes the probability that a UN (SN) possesses l connections. Polynomial representations of these degree distributions are given by

$$\Lambda(x)=\sum_l \Lambda_l x^l \quad \text{and} \quad \text{P}(x)=\sum_l \text{P}_l x^l, \tag{15}$$

respectively, and we also define the edge-perspective UN degree and SN degree distributions as follows

$$\lambda(x)=\sum_l \lambda_l x^{l-1} \quad \text{and} \quad \rho(x)=\sum_l \rho_l x^{l-1}, \tag{16}$$

where λ_l (ρ_l) denotes the probability that an edge is connected to a degree-l UN (SN). The probabilities λ_l and ρ_l are given by

$$\lambda_l=\frac{l\Lambda_l}{\sum l\Lambda_l} \quad \text{and} \quad \rho_l=\frac{l\text{P}_l}{\sum l\text{P}_l}. \tag{17}$$

and we can derive that $\lambda(x)=\Lambda'(x)/\Lambda'(1)$ and $\rho(x)=\text{P}'(x)/\text{P}'(1)$ with Eq. (15), (16) and (17).

Generally speaking, the optimal $\Lambda(x)$ in asymptotic conditions can be found using differential evolution [11], and the entire check matrix $H*$ can be determined with the PEG algorithm and some improved algorithms [27], [28], where $\Phi(x)$ is also determined. It should be noted that the optimal degree distribution obtained in [11] is suitable for a single frame without coupling. For the G-SC-2 and G-SC-F, a new DE is required to determine the optimal degree distribution.

In this section, we propose to use the standard πSC-IRSA to analyze the asymptotic performance of G-SC-IRSA under a standard random access model, where each activated UE randomly selects the number of packet replicas according to $\Lambda(x)$ and TSS with a uniform distribution. Note that the πSC-IRSA is determined by the parameter group $(N, M, \pi, \Lambda(x), l_c, l_d)$, where $N, M, l_d \to \infty$, l_c corresponds to two settings marked as SC-2 and SC-F, and π is used to characterize the proportion of coupled UNs in all UNs in a frame.

B. Degree Distribution of SC-2

In this subsection, we derive the degree distribution of SC-2. Firstly, we divide the nodes into four sets, denoted as $\mathcal{U}_1$ and $\mathcal{U}_2$ UNs in the first and second frames, respectively, and $\mathcal{S}_1$ and $\mathcal{S}_2$ SNs in the first and second frames, respectively. Note that the number of *activated* UN is $\mathbb{E}[N_a]=\pi N$ per frame, i.e., $2\pi N$ per coupled frame, and the number of coupled activated UN (C-UN) is $N_C=\pi^2 N$ in coupled frame. Then, we divide UN in the first frame into C-UN and uncoupled activated UN (UC-UN), marked by $\mathcal{U}_1^c, \mathcal{U}_1^{\bar{c}} \in \mathcal{U}_1$. These five types of nodes are shown in Fig. 8, with the bipartite graph of the G-SC-IRSA. Note that only $\pi^2 N$ UNs are C-UNs, and are all in the first frame, while the coupled SNs are all in the second frame. Accordingly, we define the node-perspective UN degree distribution for πSC-IRSA as follows

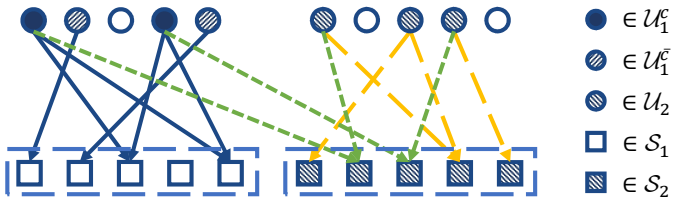

Fig. 8. Node set partitioning for SC-2. There are $2N$ UNs and $2M$ SNs in the figure, where the number of activated UN is determined by the activation probability π, and the average size of the set associated with UN is that, $|\mathcal{U}_2|=\pi N$, $|\mathcal{U}_1^c|=\pi^2 N$ and $|\mathcal{U}_1^{\bar{c}}|=\pi(1-\pi)N$.

$$\begin{cases} \Lambda^{\mathcal{U}_1^c\to\mathcal{S}_2}(x)=x, & (18)\\ \Lambda^{u_1\to\mathcal{S}_1}(x)=\sum_l \Lambda^{u_1\to\mathcal{S}_1}x^l=\sum_l \Lambda_l x^l, & (19)\\ \Lambda^{\mathcal{U}_2\to\mathcal{S}_2}(x)=\sum_l \Lambda^{\mathcal{U}_2\to\mathcal{S}_2}x^l=\sum_l \Lambda_l x^l, & (20)\end{cases}$$

where Eq. (18) means that all C-UNs must be connected to SN in set $\mathcal{S}_2$, and $u_1 \in \{\mathcal{U}_1^c, \mathcal{U}_1^{\bar{c}}\}$ in Eq. (19) represents all UNs in the first frame. Eq. (19) and (20) represents that there are the same degree distribution in edges $u_1 \to \mathcal{S}_1$ and $\mathcal{U}_2 \to \mathcal{S}_2$. The corresponding edge-perspective UN degree distributions are

$$\begin{cases} \lambda^{\mathcal{U}_1^c\to\mathcal{S}_2}(x)=1, & (21)\\ \lambda^{u_1\to\mathcal{S}_1}(x)=\sum_l \lambda_l x^{l-1}, & (22)\\ \lambda^{\mathcal{U}_2\to\mathcal{S}_2}(x)=\sum_l \lambda_l x^{l-1}. & (23)\end{cases}$$

Correspondingly, we define the node-perspective SN degree distribution for πSC-IRSA are

$$\begin{cases} \text{P}^{\mathcal{S}_2\to\mathcal{U}_1^c}(x)=\sum_{l_0} \text{P}_{l_0}^{\mathcal{S}_2\to\mathcal{U}_1^c}x^{l_0}, & (24)\\ \text{P}^{\mathcal{S}_i\to\mathcal{U}_i}(x)=\sum_l \text{P}_l^{\mathcal{S}_i\to\mathcal{U}_i}x^l, & (25)\end{cases}$$

where $i \in \{1,2\}$ in this subsection, and the corresponding edge-perspective degree distributions are

$$\begin{cases} \rho^{\mathcal{S}_2\to\mathcal{U}_1^c}(x)=\dfrac{(\text{P}^{\mathcal{S}_2\to\mathcal{U}_1^c})'(x)}{(\text{P}^{\mathcal{S}_2\to\mathcal{U}_1^c})'(1)}=\sum_{l_0}\rho_{l_0}^{\mathcal{S}_2\to\mathcal{U}_1^c}x^{l_0}, & (26)\\ \rho^{\mathcal{S}_i\to\mathcal{U}_i}(x)=\dfrac{(\text{P}^{\mathcal{S}_i\to\mathcal{U}_i})'(x)}{(\text{P}^{\mathcal{S}_i\to\mathcal{U}_i})'(1)}=\sum_l \rho_l^{\mathcal{S}_i\to\mathcal{U}_i}x^l. & (27)\end{cases}$$

We first derive $\text{P}_{l_0}^{\mathcal{S}_2\to\mathcal{U}_1^c}$, which is the degree distribution of cross edges. Denote L_0 as the average number of edges between $\mathcal{S}_2$ and $\mathcal{U}_1^c$. Clearly, one C-UN connects one edge to 2-SN with probability $1/M$, and there are total πN_a C-UNs, which means L_0 follows the Binomial distribution with

$(\pi N_a, 1/M)$. When $N, M \to \infty$, L_0 follows the Poisson distribution with πG, and we have

$$\mathrm{P}_{l_0}^{\mathcal{S}_2\to\mathcal{U}_1^c} = \Pr\{L_0 = l_0\} = \exp(-\pi G)\frac{(\pi G)^{l_0}}{l_0!}. \tag{28}$$

Thus, we can derive the node-perspective SN degree distribution $\mathrm{P}^{\mathcal{S}_2\to\mathcal{U}_1}(x)$ as

$$\begin{aligned}\mathrm{P}^{\mathcal{S}_2\to\mathcal{U}_1^c}(x) &= \sum_{l_0}\mathrm{P}_{l_0}^{\mathcal{S}_2\to\mathcal{U}_1^c}x^{l_0}\\ &= \sum_{l_0}\exp(\pi G)\frac{(\pi G)^{l_0}}{l_0!}x^{l_0}\\ &= \exp(-\pi G(1-x)).\end{aligned} \tag{29}$$

Similarly, we can derive $\mathrm{P}^{\mathcal{S}_i\to\mathcal{U}_i}(x), i = 1, 2$, because these two degree distribution are the same with $\mathrm{P}(x)$, which is the degree distribution of SN in a single frame without coupling. Let l denote the average number of edges connected to one SN inside the first or second frame, and the probability of an edge connected to a SN is $1/M$. There are total $N_a\Lambda'(1)$ edges from UNs, which means l follows the Binomial distribution with $(N_a\Lambda'(1), 1/M)$. When $N, M \to \infty$, l follows the Poisson distribution with $(G\Lambda'(1))$, thus, we have

$$\mathrm{P}_l = \Pr\{L = l\} = \exp(-G\Lambda'(1))\frac{(G\Lambda'(1))^l}{l!}, \tag{30}$$

and $\mathrm{P}^{\mathcal{S}_i\to\mathcal{U}_i}(x)$ can be derived as following

$$\begin{aligned}\mathrm{P}^{\mathcal{S}_i\to\mathcal{U}_i}(x) = \mathrm{P}(x) &= \sum_{l}\mathrm{P}_l x^l\\ &= \sum_{l}\exp(G\Lambda'(1))\frac{(G\Lambda'(1))^l}{l!}x^l\\ &= \exp(-G\Lambda'(1)(1-x)).\end{aligned} \tag{31}$$

The edge-perspective SN degree distribution is as follows

$$\begin{cases}\rho^{\mathcal{S}_2\to\mathcal{U}_1^c}(x) = \exp(-\pi G(1-x)), & (32)\\ \rho^{\mathcal{S}_i\to\mathcal{U}_i}(x) = \exp(-G\Lambda'(1)(1-x)). & (33)\end{cases}$$

C. Degree Distribution of SC-F

In the setting of SC-F, since all frames have C-UN except the last frame, we assume that there are total K frames, and use the subscript k to represent the k-th frame. First, the UN and SN are divided into K sets according to the index of frames, labeled as $\mathcal{U}_k$ and $\mathcal{S}_k$, where $k = 1, 2, \ldots, K$. Then, divide the first $K-1$ set $\mathcal{U}_k$ into $2K-2$ sets according to C-UN and UC-UN, where the set of C-UN in the k-th frame is marked by $\mathcal{U}_k^c$, and the set of UC-UN is marked by $\mathcal{U}_k^{\bar{c}}$. The set of UN and SN for SC-F is shown in Fig. 9. It can be seen that although there are more sets, the edge connection relationship between sets is not much different from SC-2.

We first give the node-perspective UN degree distribution of SC-F. Each C-UN in the set $\mathcal{U}_i^c$ provides a cross edge to the SN in the next frame, which means

$$\Lambda^{\mathcal{U}_k^c\to\mathcal{S}_{k+1}}(x) = x, \quad k = 1, 2, \ldots, K-1. \tag{34}$$

Inside the frame, the edges connected from the three types of UNs, i.e., $\mathcal{U}_k^c \to \mathcal{S}_k, \mathcal{U}_k^{\bar{c}} \to \mathcal{S}_k$ and $\mathcal{U}_K \to \mathcal{S}_K$, have nothing to do with the coupling, and they all have the same degree distribution. Thus, the node-perspective UN degree distribution for these three type set are

$$\Lambda^{u_k\to\mathcal{S}_k}(x) = \sum_l \Lambda_l x^l, \tag{35}$$

for $u_k \in \{\mathcal{U}_k^c, \mathcal{U}_k^{\bar{c}}\}$, where $k = 1, 2, \ldots, K-1$, and

$$\Lambda^{\mathcal{U}_K\to\mathcal{S}_K}(x) = \sum_l \Lambda_l x^l. \tag{36}$$

The edge-perspective UN degree distribution corresponding to the above four types of UN is as follows,

$$\begin{cases}\lambda^{\mathcal{U}_k^c\to\mathcal{S}_{k+1}}(x) = 1, & (37)\\ \lambda^{u_k\to\mathcal{S}_k}(x) = \sum_l \lambda_l x^{l-1}, & (38)\\ \lambda^{\mathcal{U}_K\to\mathcal{S}_K}(x) = \sum_l \lambda_l x^{l-1}. & (39)\end{cases}$$

For the SN in SC-F except $\mathcal{S}_1$, there are two types of edges, cross edges and internal edges. Both types of edges have exactly the same behavior as the edges in SC-2, thus the node-perspective SN degree distribution can be derived as follows,

$$\begin{cases}\mathrm{P}^{\mathcal{S}_{k+1}\to\mathcal{U}_k^c}(x) = \exp(-\pi G(1-x)), & (40)\\ \mathrm{P}^{\mathcal{S}_{k+1}\to\mathcal{U}_{k+1}}(x) = \exp(-G\Lambda'(1)(1-x)), & (41)\end{cases}$$

where $k = 1, 2, \ldots, K-1$. Note that we use subscript $k+1$ in Eq. (41) instead of k to match with Eq. (40), and for $\mathcal{S}_1$, we also have,

$$\mathrm{P}^{\mathcal{S}_1\to\mathcal{U}_1}(x) = \exp(-G\Lambda'(1)(1-x)). \tag{42}$$

The corresponding edge-perspective SN degree distribution are as follows,

$$\begin{cases}\rho^{\mathcal{S}_{k+1}\to\mathcal{U}_k^c}(x) = \mathrm{P}^{\mathcal{S}_{k+1}\to\mathcal{U}_k^c}(x) = \exp(-\pi G(1-x)), & (43)\\ \rho^{\mathcal{S}_{k+1}\to\mathcal{U}_{k+1}}(x) = \mathrm{P}^{\mathcal{S}_{k+1}\to\mathcal{U}_{k+1}}(x) = \rho^{\mathcal{S}_1\to\mathcal{U}_1}(x)\\ \qquad = \mathrm{P}^{\mathcal{S}_1\to\mathcal{U}_1}(x) = \exp(-G\Lambda'(1)(1-x)), & (44)\end{cases}$$

D. Density Evolution of SC-2

In the asymptotic analysis, πSC-IRSA exhibits a threshold effect, where all packet replicas can be decoded by SIC when the system load is less than a threshold. We derive DE to calculate this threshold load, denoted as G^*.

Based on the above five sets mentioned in Fig. 8, we define the following seven types of erasure probabilities as shown in Fig. 10, such as $p_{\mathcal{U}_1^c\to\mathcal{S}_1}$, $p_{\mathcal{U}_1^{\bar{c}}\to\mathcal{S}_1}$, $p_{\mathcal{U}_2\to\mathcal{S}_2}$, $p_{\mathcal{U}_1^c\to\mathcal{S}_2}$, $q_{\mathcal{S}_1\to\mathcal{U}_1}$, $q_{\mathcal{S}_2\to\mathcal{U}_2}$ and $q_{\mathcal{S}_2\to\mathcal{U}_1^c}$, where $p_{\mathcal{U}_1^c\to\mathcal{S}_1}$ denotes the erasure probability from a C-UN in the first frame to a SN in the first frame, and so on.

We first derive $p_{\mathcal{U}_1^c\to\mathcal{S}_2}$ and $p_{\mathcal{U}_1^{\bar{c}}\to\mathcal{S}_1}$. For an UN, if all incoming messages are erased, one outgoing message from it is erased. For a C-UN in the set $\mathcal{U}_1^c$, there are l internal edges, marked as $\{e_1, e_2, \ldots, e_l\} \in \mathcal{E}$, and a cross edge connected to $\mathcal{S}_2$, marked as e_0. All edges in the set $\mathcal{E}$ have the same erasure probability, i.e., $q_{\mathcal{S}_1\to\mathcal{U}_1}$. The erasure probability of outgoing

This article has been accepted for publication in IEEE Internet of Things Journal. This is the author's version which has not been fully edited and content may change prior to final publication. Citation information: DOI 10.1109/JIOT.2022.3232568

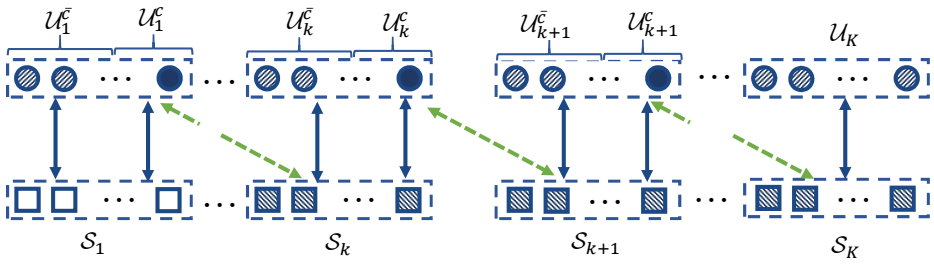

Fig. 9. Node set partitioning in the SC-F setting. There are NK UNs and MK SNs in the figure, where the number of activated UN in a frame is also determined by the activation probability π, and the average size of the set associated with UN is that, $|\mathcal{U}_K| = \pi N$, $|\mathcal{U}_k^c| = \pi^2 N$ and $|\mathcal{U}_k^{\bar{c}}| = \pi(1-\pi)N$ with $k = 1, 2, \ldots, K-1$. The cross edges are marked with dashed lines, and the interior edges with solid lines. There are two types of interior edges in the first $K-1$ frames and only one type in the K-th frame.

message along the edge e_0 is the one that all the edges in the set $\mathcal{E}$ are erased. Thus, $p_{\mathcal{U}_1^c \to \mathcal{S}_2}$ can be derived as,

$$p_{\mathcal{U}_1^c \to \mathcal{S}_2} = \sum_l \Lambda_l (q_{\mathcal{S}_1 \to \mathcal{U}_1})^l = \Lambda(q_{\mathcal{S}_1 \to \mathcal{U}_1}). \tag{45}$$

On the other hand, the erasure probability of the outgoing message along an internal edge e_i can be expressed as the probability that the remaining $l-1$ edges in the set $\mathcal{E}$ and a cross edge e_0 are erased. With the node-perspective UN degree distribution, $p_{\mathcal{U}_1^{\bar{c}} \to \mathcal{S}_1}$ is obtained as,

$$p_{\mathcal{U}_1^{\bar{c}} \to \mathcal{S}_1} = q_{\mathcal{S}_2 \to \mathcal{U}_1^c} \sum_l \Lambda_l (q_{\mathcal{S}_1 \to \mathcal{U}_1})^{l-1} = q_{\mathcal{S}_2 \to \mathcal{U}_1} \lambda(q_{\mathcal{S}_1 \to \mathcal{U}_1}). \tag{46}$$

In a similar way, $p_{\mathcal{U}_1^{\bar{c}} \to \mathcal{S}_1}$ and $p_{\mathcal{U}_2 \to \mathcal{S}_2}$ can be derived by analyzing the edge of UC-UN in set $\mathcal{U}_1^{\bar{c}}$ and $\mathcal{U}_2$, and we have,

$$\begin{cases} p_{\mathcal{U}_1^{\bar{c}} \to \mathcal{S}_1} = \lambda(q_{\mathcal{S}_1 \to \mathcal{U}_1}), & (47) \\ p_{\mathcal{U}_2 \to \mathcal{S}_2} = \lambda(q_{\mathcal{S}_2 \to \mathcal{U}_2}). & (48) \end{cases}$$

Then, we derive $q_{\mathcal{S}_2 \to \mathcal{U}_1}$, $q_{\mathcal{S}_2 \to \mathcal{U}_2}$ and $q_{\mathcal{S}_1 \to \mathcal{U}_1}$. For a SN, if at least one of its incoming messages is erased, one outgoing message from it is erased. Consider a SN in set $\mathcal{S}_2$, there are also two types of edges, one type of edge is connected to $\mathcal{U}_1^c$, belongs to $\mathcal{E}_{\rm c}$, called cross edge. The other type of edge is connected to $\mathcal{U}_2$, called internal edge, belongs to $\mathcal{E}_{\rm in}$. We suppose that there are l internal edges in $\mathcal{E}_{\rm in}$, l_0 cross edges in $\mathcal{E}_{\rm c}$ as shown in Fig. 10. Then, the probability that an outgoing message along an edge $e_c \in \mathcal{E}_{\rm c}$ is not erased, $\bar{p}_c$, is the probability that none of the remaining $l_0 - 1$ edges in set $\mathcal{E}_{\rm c} \backslash e_c$ and none of the l edges in set $\mathcal{E}_{\rm in}$ are erased, i.e., $\bar{p}_c = (1 - p_{\mathcal{U}_1^c \to \mathcal{S}_2})^{l_0 - 1}(1 - p_{\mathcal{U}_2 \to \mathcal{S}_2})^l$. Thus the erasure probability of an outgoing message along an edge $e_c \in \mathcal{E}_{\rm c}$ is that $p_c = 1 - (1 - p_{\mathcal{U}_1^c \to \mathcal{S}_2})^{l_0 - 1}(1 - p_{\mathcal{U}_2 \to \mathcal{S}_2})^l$. Let $(1 - p_{\mathcal{U}_1^c \to \mathcal{S}_2})^{l_0 - 1}$ average through the edge-perspective UN degree distribution $\rho^{\mathcal{S}_2 \to \mathcal{U}_1^c}(x)$, and $(1 - p_{\mathcal{U}_2 \to \mathcal{S}_2})^l$ average through the node-perspective UN degree distribution $\mathrm{P}^{\mathcal{S}_2 \to \mathcal{U}_2}(x)$, $q_{\mathcal{S}_2 \to \mathcal{U}_1^c}$ is obtained as,

$$\begin{aligned} q_{\mathcal{S}_2 \to \mathcal{U}_1^c} &= 1 - \left(\sum_{l_0 = 1} \rho_{l_0}^{\mathcal{S}_2 \to \mathcal{U}_1^c} (1 - p_{\mathcal{U}_1^c \to \mathcal{S}_2})^{l_0 - 1} \right) \times \\ &\quad \left(\sum_{l=0} \mathrm{P}_l^{\mathcal{S}_2 \to \mathcal{U}_2} (1 - p_{\mathcal{U}_2 \to \mathcal{S}_2})^l \right) \\ &\triangleq 1 - \left(\sum_{l_0 = 0} \mathrm{P}_{l_0}^{\mathcal{S}_2 \to \mathcal{U}_1^c} (1 - p_{\mathcal{U}_1^c \to \mathcal{S}_2})^{l_0} \right) \times \\ &\quad \mathrm{P}^{\mathcal{S}_2 \to \mathcal{U}_2} (1 - p_{\mathcal{U}_2 \to \mathcal{S}_2}) \\ &= 1 - \mathrm{P}^{\mathcal{S}_2 \to \mathcal{U}_1^c} (1 - p_{\mathcal{U}_1^c \to \mathcal{S}_2}) \mathrm{P}^{\mathcal{S}_2 \to \mathcal{U}_2} (1 - p_{\mathcal{U}_2 \to \mathcal{S}_2}) \\ &= 1 - \exp(-G(\pi p_{\mathcal{U}_1^c \to \mathcal{S}_2} + \Lambda'(1) p_{\mathcal{U}_2 \to \mathcal{S}_2})), \end{aligned} \tag{49}$$

where in (Δ) we used $\rho_{l_0}^{\mathcal{S}_2 \to \mathcal{U}_1^c} = \mathrm{P}_{l_0}^{\mathcal{S}_2 \to \mathcal{U}_1^c}$, and let $l_0 \leftarrow l_0 - 1$. Similarly, $q_{\mathcal{S}_2 \to \mathcal{U}_2}$ can be derived as

$$\begin{aligned} q_{\mathcal{S}_2 \to \mathcal{U}_2} &= 1 - \left(\sum_{l_0 = 0} \mathrm{P}_{l_0}^{\mathcal{S}_2 \to \mathcal{U}_1^c} (1 - p_{\mathcal{U}_1^c \to \mathcal{S}_2})^{l_0} \right) \times \\ &\quad \left(\sum_{l=1} \rho_l^{\mathcal{S}_2 \to \mathcal{U}_2} (1 - p_{\mathcal{U}_2 \to \mathcal{S}_2})^{l-1} \right) \\ &= 1 - \exp(-G(\pi p_{\mathcal{U}_1^c \to \mathcal{S}_2} + \Lambda'(1) p_{\mathcal{U}_2 \to \mathcal{S}_2})). \end{aligned} \tag{50}$$

Note that $q_{\mathcal{S}_2 \to \mathcal{U}_1^c} = q_{\mathcal{S}_2 \to \mathcal{U}_2}$ with the fact $\mathrm{P}^{\mathcal{S}_2 \to \mathcal{U}_1^c}(x) = \rho^{\mathcal{S}_2 \to \mathcal{U}_1^c}(x)$ and $\mathrm{P}^{\mathcal{S}_2 \to \mathcal{U}_2}(x) = \rho^{\mathcal{S}_2 \to \mathcal{U}_2}(x)$.

Finally, we consider a SN in the set $\mathcal{S}_1$. The incoming messages have two different erasure probabilities from two types of UN. Denote the edge from $\mathcal{U}_1^c$ by $\mathcal{E}_{\rm c}$ and edge from $\mathcal{U}_1^{\bar{c}}$ by $\mathcal{E}_{\rm uc}$, where the number of these two type edges account for π and $1 - \pi$ of the total number of edges. Thus we can derive the erasure probability of an outgoing message along an edge $e \in \{\mathcal{E}_{\rm c}, \mathcal{E}_{\rm uc}\}$ as follows,

$$\begin{aligned} p_e &= 1 - (1 - p_{\mathcal{U}_1^c \to \mathcal{S}_1})^{\pi(l-1)} (1 - p_{\mathcal{U}_1^{\bar{c}} \to \mathcal{S}_1})^{(1-\pi)(l-1)} \\ &= 1 - \left((1 - p_{\mathcal{U}_1^c \to \mathcal{S}_1})^{\pi} (1 - p_{\mathcal{U}_1^{\bar{c}} \to \mathcal{S}_1})^{(1-\pi)} \right)^{l-1} \end{aligned} \tag{51}$$

where $l - 1$ represents the remaining edges in $\mathcal{E}$ and marked $\bar{p}_0 = (1 - p_{\mathcal{U}_1^c \to \mathcal{S}_1})^{\pi} (1 - p_{\mathcal{U}_1^{\bar{c}} \to \mathcal{S}_1})^{(1-\pi)}$. Let $\bar{p}_0$ average through the edge-perspective UN degree distribution $\rho^{\mathcal{S}_1 \to \mathcal{U}_1}(x)$, $q_{\mathcal{S}_1 \to \mathcal{U}_1}$ can be derived as follows,

$$\begin{aligned} q_{\mathcal{S}_1 \to \mathcal{U}_1} &= 1 - \sum_{l=1} \rho_l^{\mathcal{S}_1 \to \mathcal{U}_1} (\bar{p}_0)^{l-1} \\ &= 1 - \rho^{\mathcal{S}_1 \to \mathcal{U}_1}(\bar{p}_0) \\ &= 1 - \exp(-G\Lambda'(1) \tilde{p}_{\mathcal{U}_1 \to \mathcal{S}_1}), \end{aligned} \tag{52}$$

where

$$\begin{aligned} \tilde{p}_{\mathcal{U}_1 \to \mathcal{S}_1} &= 1 - \bar{p}_0 \\ &= 1 - (1 - p_{\mathcal{U}_1^c \to \mathcal{S}_1})^{\pi} (1 - p_{\mathcal{U}_1^{\bar{c}} \to \mathcal{S}_1})^{(1-\pi)}. \end{aligned} \tag{53}$$

This article has been accepted for publication in IEEE Internet of Things Journal. This is the author's version which has not been fully edited and content may change prior to final publication. Citation information: DOI 10.1109/JIOT.2022.3232568

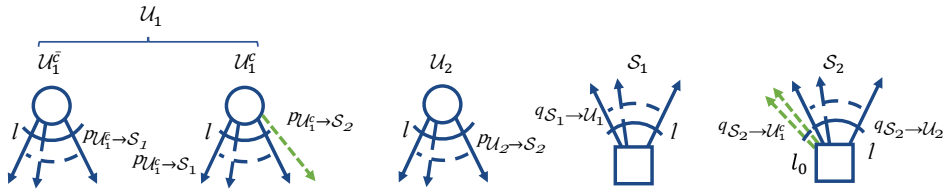

Fig. 10. Five types of nodes and their corresponding connectivity in SC-2 case.

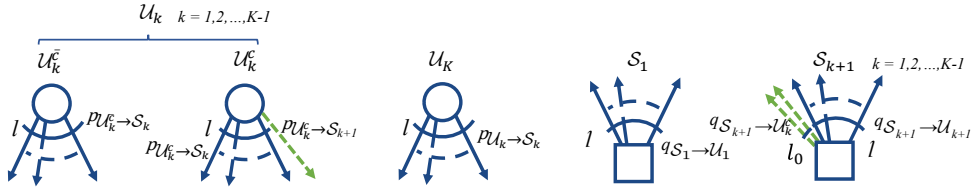

Fig. 11. Five types of nodes and their corresponding connectivity in SC-F case.

According to the distribution of UN and the iterative update process of erasure probability, the average erasure probability of UN in the t-th iteration $\bar{p}^{(t)}$ can be calculated as:

$$\begin{aligned}\bar{p}^{(t)} =&\frac{\pi}{2}\Lambda(q^{(t)}_{\mathcal{S}_1\to\mathcal{U}_1})q^{(t)}_{\mathcal{S}_2\to\mathcal{U}_1^c}+\frac{1}{2}\Lambda(q^{(t)}_{\mathcal{S}_2\to\mathcal{U}_2})\\&+\frac{1}{2}(1-\pi)\Lambda(q^{(t)}_{\mathcal{S}_1\to\mathcal{U}_1}).\end{aligned}\tag{54}$$

The iterative process of DE starts with $p_{\mathcal{U}_1^c\to\mathcal{S}_1}$, $p_{\mathcal{U}_1^{\bar{c}}\to\mathcal{S}_1}$, $p_{\mathcal{U}_2\to\mathcal{S}_2}$, $p_{\mathcal{U}_1^c\to\mathcal{S}_2}$, $q_{\mathcal{S}_1\to\mathcal{U}_1}$, $q_{\mathcal{S}_2\to\mathcal{U}_2}$ and $q_{\mathcal{S}_1\to\mathcal{U}_1}$ initialized to 1, which means all UNs are unknown, and updates (45)-(53) iteratively. The threshold load G^* is the largest value of G, where $\bar{p}$ converges to 0.

E. Density Evolution of SC-F

As shown in Fig. 11, there are also five types of nodes and seven types of erasure probabilities in bipartite graph for the setting SC-F. For the erasure probability along the edges from UNs, we can find the same structure (same edges and their connection relationship) in SC-2, so we obtain these erasure probabilities in the same way and show as following,

$$\begin{cases}p_{\mathcal{U}_k^c\to\mathcal{S}_{k+1}}=\Lambda(q_{\mathcal{S}_k\to\mathcal{U}_k}), &(55)\\ p_{\mathcal{U}_k^c\to\mathcal{S}_k}=q_{\mathcal{S}_{k+1}\to\mathcal{U}_k^c}\lambda(q_{\mathcal{S}_k\to\mathcal{U}_k}), &(56)\\ p_{\mathcal{U}_k^{\bar{c}}\to\mathcal{S}_k}=\lambda(q_{\mathcal{S}_k\to\mathcal{U}_k}), &(57)\\ p_{\mathcal{U}_K\to\mathcal{S}_K}=\lambda(q_{\mathcal{S}_K\to\mathcal{U}_K}), &(58)\end{cases}$$

where $k=1,2,\ldots,K-1$.

For the erasure probability along the edges from $\mathcal{S}_1$, it is the same with Eq. (52). For the erasure probabilities along the edges from $\mathcal{S}_{k+1}$ where $k=1,2,\ldots,K-2$, there are 3 type of edges from $\mathcal{U}_{k+1}^c$,$\mathcal{U}_{k+1}^{\bar{c}}$ and $\mathcal{U}_k^c$, using the method to obtain the $q_{\mathcal{S}_1\to\mathcal{U}_1}$ and $q_{\mathcal{S}_2\to\mathcal{U}_2}$, $q_{\mathcal{S}_{k+1}\to\mathcal{U}_{k+1}}$ can be expressed as

$$\begin{aligned}q_{\mathcal{S}_{k+1}\to\mathcal{U}_{k+1}}=1-\exp(-G(&\pi p_{\mathcal{U}_k^c\to\mathcal{S}_{k+1}}\\&+\Lambda'(1)\tilde{p}_{\mathcal{U}_{k+1}\to\mathcal{S}_{k+1}})),\end{aligned}\tag{59}$$

TABLE I
OPTIMAL DEGREE DISTRIBUTION FOR SC-2 SETTING

Label	G^*	$\Lambda(x)$
$Lt4$	0.868	$0.482x^4+0.518x^2$
$Lt5$	0.904	$0.378x^5+0.622x^2$
$Lt6$	0.929	$0.332x^6+0.668x^2$
$Lt8$	0.943	$0.249x^8+0.168x^3+0.583x^2$
$Lt12$	0.958	$0.176x^{12}+0.393x^3+0.431x^2$

TABLE II
OPTIMAL DEGREE DISTRIBUTION FOR SC-F SETTING

Label	G^*	$\Lambda(x)$
$La4$	0.866	$0.455x^4+0.545x^2$
$La5$	0.898	$0.365x^5+0.635x^2$
$La6$	0.913	$0.320x^6+0.058x^3+0.622x^2$
$La8$	0.932	$0.223x^8+0.212x^3+0.565x^2$
$La12$	0.952	$0.169x^{12}+0.360x^3+0.471x^2$

where

$$\tilde{p}_{\mathcal{U}_{k+1}\to\mathcal{S}_{k+1}}=1-(1-p_{\mathcal{U}_{k+1}^c\to\mathcal{S}_{k+1}})^{\pi}(1-p_{\mathcal{U}_{k+1}^{\bar{c}}\to\mathcal{S}_{k+1}})^{(1-\pi)}.\tag{60}$$

We can also obtain $q_{\mathcal{S}_{k+1}\to\mathcal{U}_k^c}$ because of $q_{\mathcal{S}_{k+1}\to\mathcal{U}_k^c}=q_{\mathcal{S}_{k+1}\to\mathcal{U}_{k+1}}$ with the suppose of Poisson distribution in both node and edge perspective SN degree distribution.

In $\mathcal{S}_K$, these two erasure probabilities mentioned above can be calculated by

$$\begin{aligned}q_{\mathcal{S}_K\to\mathcal{U}_K}&=q_{\mathcal{S}_K\to\mathcal{U}_{K-1}^c}\\&=1-\exp(-G(\pi p_{\mathcal{U}_{K-1}^c\to\mathcal{S}_K}+\Lambda'(1)p_{\mathcal{U}_K\to\mathcal{S}_K})).\end{aligned}\tag{61}$$

Then, the DE is performed similarly to SC-2 by iteratively updating Eq. (55)-(61), with these erasure probabilities initialized to 1. The PLR in the t-th iteration $\bar{p}^{(t)}$ can be calculated

This article has been accepted for publication in IEEE Internet of Things Journal. This is the author's version which has not been fully edited and content may change prior to final publication. Citation information: DOI 10.1109/JIOT.2022.3232568

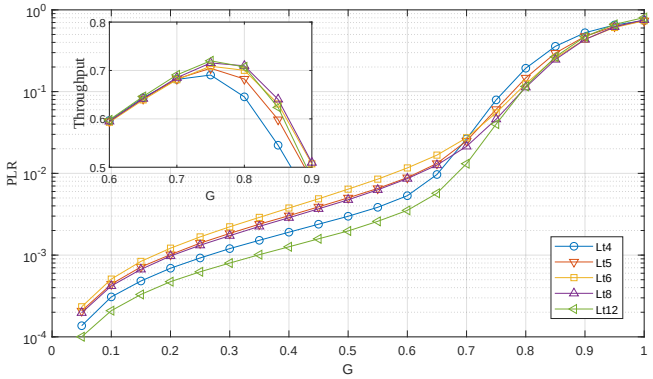

(a) PLR and throughput performance for SC-2 setting.

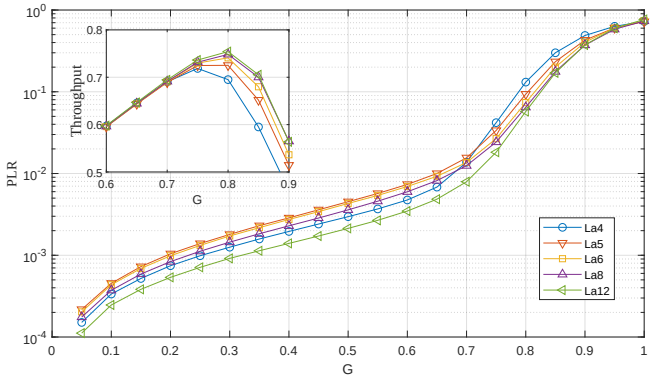

(b) PLR and throughput performance for SC-F setting.

Fig. 12. The PLR and throughput performance for SC-2 and SC-F setting using optimal degree distribution mentioned in Table I and Table II with limited $d_{\max}$ versus the system load G. The simulation is carried out with the number of UEs $N = 2000$, the frame length $M = 200$ and $\pi_d = 0.1$, and a total of 10^6 frames are simulated.

by

$$\bar{p}^{(t)} = \frac{1}{K}\Bigg(\pi \sum_{k=1}^{K-1} \Lambda(q^{(t)}_{\mathcal{S}_k \to \mathcal{U}_k}) q^{(t)}_{\mathcal{S}_{k+1} \to \mathcal{U}_k^c} + (1-\pi) \sum_{k=1}^{K-1} \Lambda(q^{(t)}_{\mathcal{S}_k \to \mathcal{U}_k}) + \Lambda(q^{(t)}_{\mathcal{S}_K \to \mathcal{U}_K})\Bigg). \quad (62)$$

Note that the number of frames K is approaching ∞ to obtain an exact threshold with DE, which cannot be achieved in practice. In Eq. (62), we can choose the first $K' < K$ nodes to calculate $\bar{p}$ as the system load threshold, which does not affect searching for the optimal degree distribution. We observe that when $K \approx 100$, the increase of K hardly affects the result. Thus, in the numerical result, we take $K = 100$ and assume that the accurate G^* is obtained at this time.

V. Numerical Results

In this section, we give the numerical results of PLR and throughput performance for SC-2 and SC-F, and we then give the results of PLR, throughput and AAoI performance for G-SC-2 and G-SC-F under different parameter settings. Finally, we compared the minimum AAoI of the IRSA, G-SC-2 and G-SC-F cases.

TABLE III
Degree Distribution for G-SC-2 with Difference Frame Length

Label	M	G^*	$\Lambda(x)$ and $\mathrm{P}(x)$
$Ht1$	100	0.944	$0.247x^8 + 0.188x^3 + 0.565x^2$ $0.4x^{74} + 0.6x^{73}$
$Ht2$	200	0.945	$0.249x^8 + 0.168x^3 + 0.583x^2$ $0.62x^{37} + 0.38x^{36}$
$Ht3$	500	0.945	$0.214x^8 + 0.254x^3 + 0.532x^2$ $0.152x^{15} + 0.848x^{14}$

TABLE IV
Degree Distribution for G-SC-F with Difference Frame Length

Label	M	G^*	$\Lambda(x)$ and $\mathrm{P}(x)$
$Ha1$	100	0.935	$0.225x^8 + 0.240x^3 + 0.535x^2$ $0.8x^{72} + 0.2x^{71}$
$Ha2$	200	0.934	$0.223x^8 + 0.212x^3 + 0.565x^2$ $0.5x^{36} + 0.5x^{35}$
$Ha3$	500	0.933	$0.224x^8 + 0.100x^3 + 0.676x^2$ $0.776x^{14} + 0.224x^{13}$

A. PLR and Throughput Performance for SC-2 and SC-F

Table I and II summarize the optimal degree distributions[10] for SC-2 and SC-F settings with $\pi_d = 0.1$, which is in order to distinguish from π in the activation model. We use Lt to mark the SC-2 setting and La to mark the SC-F setting. The number on the label indicates the maximum repetitions $d_{\max}$. Both tables are obtained by the DE analysis in Sec. IV and the *differential evolution* algorithm [30]. There is a key parameter π_d in DE, which is related to η. For convenience, we let $\pi_d = \eta$, where the degree distributions shown in these two tables are suitable for the case $\eta = 0.1$.[11] Meanwhile, in order to reduce the search space in differential evolution algorithm, we assume that $\Lambda(x)$ only contains three degrees: $2, 3$ and $d_{\max}$. It can be seen from the Table I and II that the probability of optimized $d_{\max}$ for SC-F is smaller than that of SC-2, because each frame is coupled with the preceding and following frames in the SC-F, which leads to a lower $d_{\max}$ to achieve a similar bipartite graph as the SC-2.

Then, we simulated the PLR and throughput performance of the SC-2 and SC-F settings under the condition of $N = 2000, M = 200$ with the SWD $l_d = 2$ as shown in Fig. 12(a) and Fig. 12(b). It can be seen that $Lt12$ ($La12$) has the best error floor, while $Lt6$ ($La6$) has the highest error floor. The curves in Fig. 12(a) and 12(b) have similar trends, and the differences in the error floor regime are not large. In fact, the $PLR \simeq 10^{-3}$ in the case of lower system load, i.e., $G = 0.3$. However, the PLR performance in the waterfall region has a clear positive correlation with $d_{\max}$, i.e., the larger $d_{\max}$ can achieve higher maximum throughput as shown in the boxes of Fig. 12(a) and 12(b). For SC-2, the maximum throughput increased from 0.68 to 0.72, while for SC-F, the maximum throughput increased from 0.72 to 0.76, where the throughput peak is shifted to the right.

[10]The optimal degree distribution satisfies, a) contains only quadratic, cubic, and highest-order terms and b) be able to maximize G^* [11], [15].

[11]In fact $\pi = G\eta$ with Eq. (13), but we most concern about the performance under high system load, where $\pi = G\eta \approx \eta$ has a little effect on DE analysis. Thus, we use π_d to represent the parameters used in optimization, which is distinguished from the actual activation probability π.

This article has been accepted for publication in IEEE Internet of Things Journal. This is the author's version which has not been fully edited and content may change prior to final publication. Citation information: DOI 10.1109/JIOT.2022.3232568

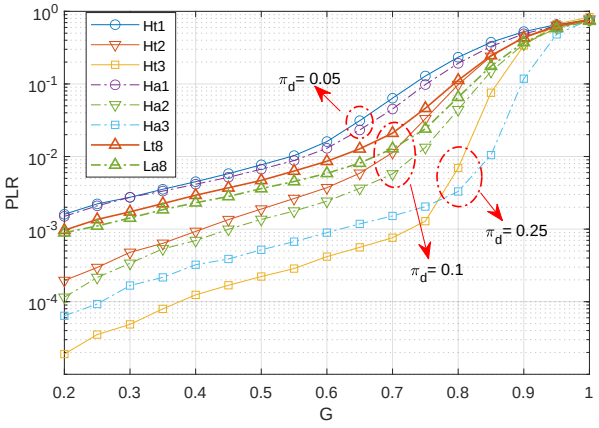

(a) The PLR versus the system load G.

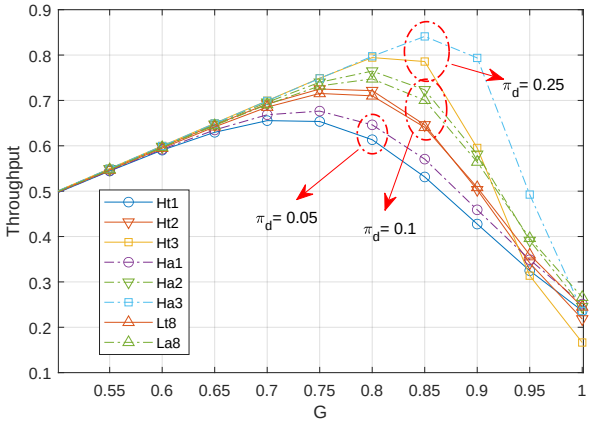

(b) Throughput versus the system load G.

Fig. 13. PLR and throughput versus the system load G for G-SC-2 and G-SC-F. The solid line represents the G-SC-2 case, while the dashed line represents the G-SC-F case. The number of UE is fixed to $N = 2000$, and we use $\circ, \triangledown, \square$ to represent the case of $M = 100, 200, 500$ respectively. These 6 cases all use different transmit matrices mentioned in Table III and IV. $Lt8$ and $La8$ are the settings of SC-2 and SC-F with the standard random access method.

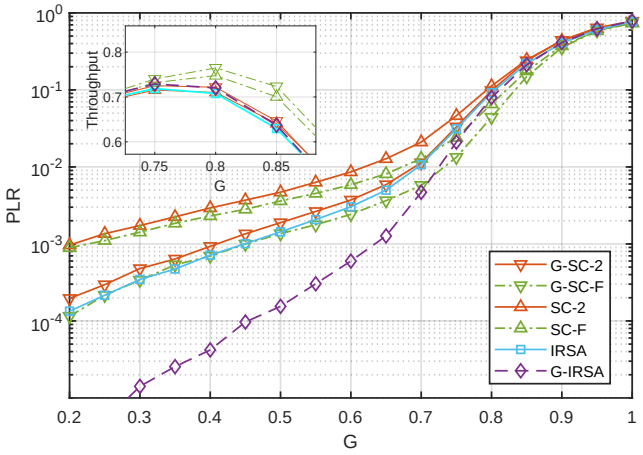

Fig. 14. PLR and throughput performance in IRSA, G-IRSA, SC-IRSA and G-SC-IRSA schemes. The degree distribution of IRSA and G-IRSA is $\lambda(x) = 0.5x^8 + 0.28x^3 + 0.22x^2$, G-SC-IRSA use $La8$ and $Lt8$. $M = 200$ and N varies according to π.

B. PLR, Throughput Performance for G-SC-2 and G-SC-F

We then present the performance of G-SC-IRSA with the optimized PRAP. At this time, the same G corresponds to different $\mathbb{E}[N_a]$, and due to the change of η, π_d also has different values. Specifically, we set $N = 2000$, and let $M = [100, 200, 500]$, which means $\pi_d = [0.05, 0.1, 0.25]$ in DE analysis. We still need to use the differential evolution algorithm to find the optimal degree distribution under different π_d, and generate the check matrix with the PEG algorithm. In order to compare with other protocol in Sec. V-D, we choose the degree distributions with $d_{\max} = 8$ to design the PRAP. Here we only record the UN(SN) degree distribution $\Lambda(x)(\mathrm{P}(x))$ corresponding to the check matrix, as shown in the Table III and IV. Note that the UN degree distribution of $Ht2$ ($Ha2$) is the same as $Lt8$ ($La8$), because of the same N, M, π_d.

The corresponding PLR and throughput performance of the G-SC-2 and G-SC-F via the PRAP with optimized degree distribution in Table III and IV are shown in Fig. 13(a) and 13(b). Specifically, the PLR of G-SC-F is lower than that of G-SC-2 in the waterfall region. This can also be seen from the trend of throughput in Fig. 13(b). When $M = 100$, the throughput of the two cases are both at $G = 0.75$, where the throughput reaches the highest point at 0.65 and 0.68, respectively. At $M = 500$, the throughput reaches the highest point with 0.785 and 0.84 respectively when $G = 0.85$. Thus, the G-SC-F has greater advantages in throughput performance. In general, the performance of G-SC-F is better than G-SC-2, where it is the opposite of the system load threshold G^* shown in Table III and IV. Since the threshold can only represent the PLR performance under the asymptotic case, it is only used as an optimization object in this paper and cannot be directly compared between different settings. In addition, we also draw the performance for SC-2 (SC-F) setting using $Lt8$ ($La8$) in the Fig. 13(a) and 13(b), and compare it to pseudo-

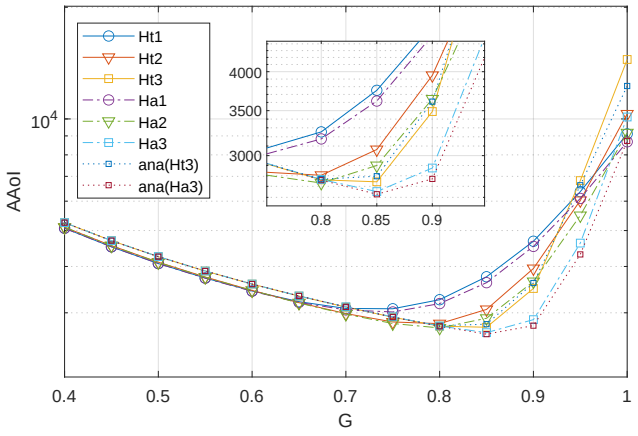

Fig. 15. AAoI performance for two case of G-SC-IRSA with different M versus the system load G. The detailed settings are the same as Fig. 13(a) and Fig. 13(b). The theoretical lines of AAoI for Ht3 and Ha3 case are also shown in the figure, where the throughput is using the data in Fig. 13(b).

random protocols with the optimized PRAP. With the same frame length $M = 200$, we can see that $Ht2$ ($Ha2$) is better than $Lt8$ ($La8$) in the most of system loads.

The throughput and PLR performance of the IRSA, G-IRSA, and G-SC-IRSA schemes are compared in Fig. 14. We can observe that the G-IRSA scheme has better error floor performance, while the SC-IRSA scheme has little improvement over the standard IRSA scheme. The throughput performance of SC-F and G-SC-F schemes are higher, while the remaining 4 protocols achieve only 0.7 of the normalized throughput.

C. AAoI Performance for G-SC-2 and G-SC-F

Recall that η affects the ratio of length to width of the check matrix, and we can obtain better PLR and throughput performance by increasing η, or M, while too long frame length M also affects the delay and timeliness of the system. To trade-off between frame length and AAoI, we show the AAoI performance under the two cases in Fig. 15. For each case, we also use the PRAP matrices mentioned in Table III and IV. It can be seen that the theoretical points and the simulation points almost coincide in Fig. 15, which verifies the correctness of our theoretical formula Eq. (11). It can also be shown by two simulation points at the same location, i.e, $G = 0.85$ to achieve the lowest AAoI in Fig. 15.

D. Minimum AAoI for G-SC-IRSA Protocol

From the above discussion, we summarize the three steps to achieve the minimum AAoI with our G-SC-IRSA protocol in the following. Without loss of generality, we assume $\eta = 0.1$ and $d_{\max} = 8$ in order to facilitate the comparison.

First, we find the optimal degree distribution that maximizes T in the asymptotic setting of SC-2 (SC-F). This is done in Sec. V-A, where the optimal degree distributions used are $Lt8$ and $La8$, respectively. Then, for the same N, we use the PEG algorithm to generate the matrix corresponding to the optimal degree distribution to determine the PRAP, denoted as P_s. In fact, we have obtained the required matrices $Ht2$ and $Ha2$ under the conditions of $N = 2000$, $\pi_d = 0.1$ and $d_{\max} = 8$.

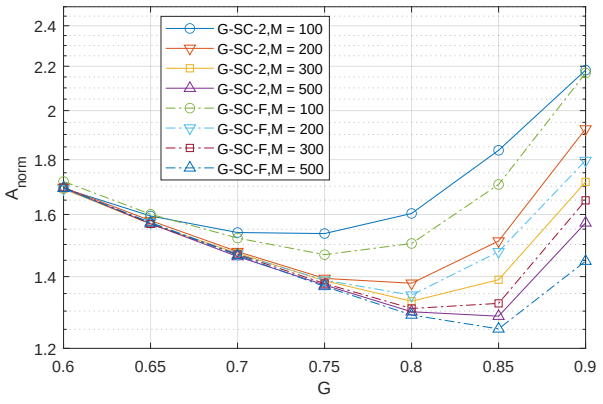

Fig. 16. Normalized AAoI A_{norm} for G-SC-IRSA with different N as well as M versus the system load G. The η is fixed to 0.1, and we mark the case $M = 100, 200, 300, 500$ as $\circ, \triangledown, \square, \triangle$,respectively. The solid line represents the G-SC-2 case, while the dashed line represents the G-SC-F case.

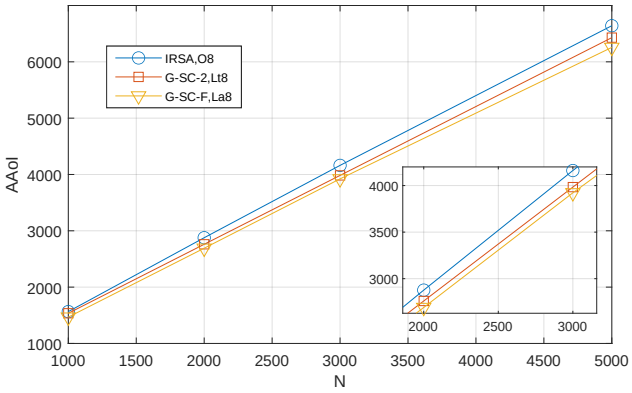

Fig. 17. Minimum AAoI achieved in IRSA and G-SC-IRSA protocol versus the number of total UEs N. The minimum AAoI is found by a grid search method with step size $\Delta G = 0.01$. The IRSA uses the $O8$ degree distribution mentioned in [26]. $Lt8$ is used for G-SC-2 case while $La8$ is used for G-SC-F case due to the same $d_{\max}$ with $O8$.

We note that these two matrices are only applicable to the case of $N = 2000$. When N changes, we need to re-use the PEG algorithm to generate the PRAP matrix. Finally, we use the grid search method on G to obtain the approximately minimum AAoI A_s in a fixed N.

Fig. 16 shows the normalized AAoI $\tilde{A}$ as a function of N, M, G, where $N = [1, 2, 3, 5] \times 10^3$ and $M = [100, 200, 300, 500]$. Since N changes in the same proportion as M, we only label M, and the step size of G is 0.05. We can observe that with the increasing of N, M, and the minimum $\tilde{A}$ shifts to the direction of high system load, and $\tilde{A}$ of G-SC-F is lower than that of G-SC-2 under most loads, which is consistent with the previous results.

Finally, we compare the minimum AAoI achieved by the standard IRSA scheme and the proposed G-SC-2 and G-SC-F schemes, as shown in Fig. 17. We can see that the minimum AAoI of the two proposed schemes is lower than that of standard IRSA, and with the increase of N, the AAoI gap between the three schemes becomes larger, indicating that our G-SC-IRSA protocol is suitable for age-critical grant-free massive access.

VI. Conclusion

In this paper, a novel G-SC-IRSA protocol has been proposed for the grant-free massive access system, in which a large number of UEs are activated randomly and generate the packets at the start of the frame. Then we describe the PRAP matrix, coupled frames, and SWD of the G-SC-IRSA protocol, and propose a framework to design the optimal PRAP matrix to enhance the PLR, throughput, and AAoI performance. Specifically, we first divide G-SC-IRSA into two typical cases, G-SC-2 and G-SC-F, and propose SC-2 and SC-F to analyze the asymptotic performance of the above cases. According to the DE analysis, we use the differential evolution algorithm to find the optimal degree distributions and finally obtain the optimal PRAP matrices. Simulation results show that our proposed G-SC-IRSA is more suitable for age-critical grant-free access while ensuring PLR and throughput.

REFERENCES

[1] J. Jiao, et al., "Massive access in space-based Internet of Things: Challenges, opportunities, and future directions," *IEEE Wireless Communications*, vol. 28, no. 5, pp. 118–125, 2021.

[2] Y. Wu, et al., "NOMA assisted multi-access mobile edge computing: A joint optimization of computation offloading and time allocation," *IEEE Transactions on Vehicular Technology*, vol. 67, no. 12, pp. 12244–12258, Dec. 2018.

[3] H. Kong, et al., "Beamforming design and performance analysis for satellite and UAV integrated networks in IoRT applications," *IEEE Internet of Things Journal*, vol. 9, no. 16, pp. 14965-14977, 2022.

[4] N. Huang, et al., "Integrated sensing and communication assisted mobile edge computing: An energy-efficient design via intelligent reflecting surface,*IEEE Wireless Communications Letters*, early access, 2022.

[5] Y. Wu, et al., "Non-orthogonal multiple access assisted federated learning via wireless power transfer: A cost-efficient approach," *IEEE Transactions on Communications*, vol. 70, no. 4, pp. 2853–2869, 2022.

[6] J. Jiao, et al., "Unequal access latency random access protocol for massive machine-type communications," *IEEE Transactions on Wireless Communications*, vol. 19, no. 9, pp. 5924–5937, 2020.

[7] J. Jiao, et al., "Intelligent hybrid nonorthogonal multiple access relaying for vehicular networks in 6G," *IEEE Internet of Things Journal*, vol. 8, no. 19, pp. 14773–14786, 2021.

[8] N. Abramson, "The throughput of packet broadcasting channels," *IEEE Transactions on Communications*, vol. 25, no. 1, pp. 117–128, 1977.

[9] Y. Wu, et al., "Massive access for future wireless communication systems," *IEEE Wireless Communications*, vol. 27, no. 4, pp. 148–156, 2020.

[10] A. Mengali, et al., "On the modeling and performance assessment of random access with SIC," *IEEE Journal on Selected Areas in Communications*, vol. 36, no. 2, pp. 292–303, 2018.

[11] G. Liva, "Graph-based analysis and optimization of contention resolution diversity slotted ALOHA," *IEEE Transactions on Communications*, vol. 59, no. 2, pp. 477–487, 2011.

[12] E. Casini, et al. "Contention resolution diversity slotted ALOHA (CRDSA): An enhanced random access scheme for satellite access packet networks," *IEEE Transactions on Wireless Communications*, vol. 6, no. 4, pp. 1408–1419, 2007.

[13] A. Graell i Amat and G. Liva, "Finite-length analysis of irregular repetition slotted ALOHA in the waterfall region," *IEEE Communications Letters*, vol. 22, no. 5, pp. 886–889, 2018.

[14] M. Ivanov, et al., "Error floor analysis of coded slotted ALOHA over packet erasure channels," *IEEE Communications Letters*, vol. 19, no. 3, pp. 419–422, 2015.

[15] E. Sandgren, et al., "On frame asynchronous coded slotted ALOHA: Asymptotic, finite length, and delay analysis," *IEEE Transactions on Communications*, vol. 65, no. 2, pp. 691–704, 2017.

[16] M. Ivanov, et al., "Broadcast coded slotted ALOHA: A finite frame length analysis," *IEEE Transactions on Communications*, vol. 65, no. 2, pp. 651–662, 2017.

[17] E. Paolini, et al., "A structured irregular repetition slotted ALOHA scheme with low error floors," in *2017 IEEE International Conference on Communications (ICC)*, 2017, pp. 1–6.

[18] G. Liva, et al., "Spatially-coupled random access on graphs," in *2012 IEEE International Symposium on Information Theory Proceedings*, 2012, pp. 478–482.

[19] J. Jiao, et al., "MSPA: Multislot pilot allocation random access protocol for mMTC-enabled IoT system," *IEEE Internet of Things Journal*, vol. 8, no. 24, pp. 17403–17416, 2021.

[20] S. Kaul, et al., "Real-time status: How often should one update?" in *Proceedings IEEE INFOCOM 2012* 2012, pp. 2731–2735.

[21] T. Yang, et al., "Grant free age-optimal random access protocol for satellite-based Internet of Things," *IEEE Transactions on Communications*, vol. 70, no. 6, pp. 3947–3961, 2022.

[22] H. Chen, et al., "Age-of-information dependent random access for massive IoT networks," *IEEE INFOCOM 2020*, 2020, pp. 930–935.

[23] O. T. Yavascan and E. Uysal, "Analysis of slotted ALOHA with an age threshold," *IEEE Journal on Selected Areas in Communications*, vol. 39, pp. 1456–1470, 2021.

[24] A. Munari and A. Frolov, "Average age of information of irregular repetition slotted ALOHA." in *IEEE Globecom 2020*, Taipei, 2020. 2020, pp. 1–6.

[25] A. Munari, "Modern random access: An age of information perspective on irregular repetition slotted ALOHA," *IEEE Transactions on Communications*, vol. 69, no. 6, pp. 3572–3585, 2021.

[26] S. Saha, et al., "On the minimum average age of information in IRSA for grant-free mMTC," *IEEE Journal on Selected Areas in Communications*, vol. 39, pp. 1441–1455, 2021.

[27] X.-Y. Hu, et al., "Irregular progressive edge-growth (PEG) tanner graphs," in *Proceedings IEEE International Symposium on Information Theory*, 2002, pp. 480–480.

[28] Z. Huang, et al., "A novel weight coefficient PEG algorithm for ultra-reliable short length analog fountain codes," *IEEE Wireless Communications Letters*, vol. 8, no. 1, pp. 125–128, 2019.

[29] A. Meloni, et al., "Sliding window-based contention resolution diversity slotted ALOHA," in *2012 IEEE Global Communications Conference (GLOBECOM)*, 2012, pp. 3305–3310.

[30] R. Storn and K. Price, "Differential evolution - a simple and efficient heuristic for global optimization over continuous spaces," *Journal of Global Optimization*, vol. 11, no. 4, pp. 341–359, 1997.